Top Catal (2011) 54:190–200
DOI 10.1007/s11244-011-9638-5

ORIGINAL PAPER

Effect of the Synthesis Method on Co-catalysts Based on MCM-41 for the Fischer–Tropsch Reaction

Andrés A. García Blanco · Ma. Gabriela Amaya · Ma. Eugenia Roca Jalil · Marcelo Nazzarro · Marcos I. Oliva · Karim Sapag

Published online: 2 February 2011

Abstract In this work, cobalt catalysts based on ordered mesoporous materials of the MCM-41 type were synthesized and characterized. The synthesis of the catalysts was performed by using different methods: impregnation; incorporation of the metal in the synthesis gel and ionic exchange of the metal by the template. Different characterization techniques were used (N_2 adsorption–desorption, XRD, TPR, SEM and XPS) to study the textural and structural properties of the samples and the metal-support interaction corresponding to each method of synthesis. These samples were tested in the CO Hydrogenation (Fischer–Tropsch Synthesis) by measuring the CO conversion and the selectivity to CO_2 and some groups of hydrocarbons chains. The results show that structural and textural properties as well as the metal-support interactions are affected by the synthesis method. According to this study, catalytic performance is related to the properties of the samples, observing that the metal support interaction highly affects the activity and selectivity of the catalysts.

Keywords Cobalt catalysts · MCM-41 · Fischer–Tropsch synthesis

A. A. García Blanco · Ma. G. Amaya · Ma. E. Roca Jalil · M. Nazzarro · K. Sapag (✉)
Laboratorio de Sólidos Porosos,
Instituto de Física Aplicada – CONICET,
Universidad Nacional de San Luis, Chacabuco 917,
5700 San Luis, Argentina
e-mail: sapag@unsl.edu.ar

M. I. Oliva
IFEG-CONICET, FaMAF Universidad Nacional de Córdoba,
Medina Allende S/N, Ciudad Universitaria, Córdoba, Argentina

1 Introduction

The production of synthetic fuels, particularly middle distillates from natural gas by the Fischer–Tropsch (FT) synthesis, has acquired a renewed interest during the last few years mainly due to the decrease of the oil reserves, the concern about the environmental effects of fuels and the availability of gas reserves [1–3].

The FT reaction consists of the catalytic CO hydrogenation from synthesis gas, a mixture rich in hydrogen and carbon monoxide (originally obtained from the charcoal gasification, but also from natural gas or biomass). This reaction produces a mixture of hydrocarbons (HC) with carbon chains corresponding to gases (from C_1 to C_4); liquids (from C_5 to C_{20}) and even waxes ($>C_{20}$), being one of the accepted mechanism the polymerization of monomers. Depending on the catalysts and process conditions [4–8], diverse HC as paraffins, olefins, alcohols, aldehydes and non desired products like CO_2 and water can be produced.

The catalysts with a high reaction performance for FT synthesis contain, as the active phase, transition metals of the group VIII, where the most used are Ruthenium (Ru), Iron (Fe), Cobalt (Co) and Nickel (Ni). Ru produces heavy HC but has the disadvantage of its limited availability and consequently being expensive; Ni exhibits a high selectivity to methane formation and Fe has several inconveniences, among them, it has a low resistance to deactivation by water and produces short HC, olefins and oxygenated compounds as well [4, 6, 7].

The Co catalysts appear to be the most suitable for producing fuels in the middle distillates range with a significant formation of *n*-paraffins, a low production of oxygenated products and a high stability to deactivation by water [9–11].

The FT catalysts are strongly influenced by the selection of their support. Among the most used supports for this kind of catalysts are: Al_2O_3 [12, 13], SiO_2 [14, 15] and TiO_2, in a lower level. The amorphous silica (SiO_2) is particularly a widely used support due to the advantage of its low interaction with the cobalt oxides, facilitating their reduction to Co^0 that is actually the active phase. However, the main problem of amorphous silica is that the particles of cobalt oxide may tend to agglomerate under the thermal treatment required for the catalyst activation, decreasing the metal dispersion and consequently, the catalyst activity per mass of active phase [3, 16–18]. A possibility to improve this fact is the use of a silica support with an important specific surface to allow a larger dispersion.

On the other hand, the growth of the HC chains during the reaction can be controlled, at first, by limiting the pore sizes of the catalyst, if the active phase is located inside the pores. From this premise, catalysts supported on porous materials such as pillared clays (PILCs) [19, 20] and ordered mesoporous materials [16, 21–24] have been widely studied in the last few years.

Mesoporous materials of the MCM-41 type are an interesting alternative to be used as supports for Co catalysts due to their textural and structural characteristics. They exhibit a hexagonal array of honeycomb-shaped unidimensional channels, well defined pore sizes between 2 and 3 nm, high surface area values (around 1000 m^2/g) and, being pure silica materials, a low interaction with cobalt [25–27].

Once the active phase and the support are selected, the synthesis procedure is also important to get the right final properties. Cobalt catalysts supported on MCM-41 have been mainly synthesized following the impregnation method [16, 28–33]. However, other methods have been also reported, such as the template-exchange method [34], the gas phase incorporation method [35] and the $Co_2(CO)_8$ impregnation from hexane solution [36].

The present work is focused on the study of the influence of the synthesis method on the textural and structural properties of Co catalysts prepared from MCM-41 mesoporous materials, as well as their catalytic activity in the Fischer–Tropsch synthesis.

2 Experimental

2.1 Sample Preparation

Co catalysts were synthesized by three methods: (i) ionic exchange of the surfactant within the MCM-41 precursor (before calcination) by Co^{2+} from the corresponding salt in solution (Co-MCM-41 EXC), (ii) impregnation of MCM-41 support with cobalt nitrate solution (Co-MCM-41 IMP) and (iii) incorporation of cobalt nitrate at the initial stage of the material synthesis (Co-MCM-41 INC).

The MCM-41 silica was prepared from a solution of NaOH, cetyl trimethyl ammonium bromide (CTAB, MERCK, ≥99.0% purity) and H_2O at a molar ratio of 0.6:0.12:100, respectively. Then 1 mol of tetraethyl orthosilicate, TEOS (MERCK, ≥99.0% purity), was added drop wise to the solution and the mixture was stirred for 24 h. Subsequently, the solid was filtered, washed with distilled water to remove the remaining surfactant and dried at 60 °C for approximately 12 h in air, obtaining the MCM-41 precursor. To obtain the MCM-41 support, the precursor was calcined at 500 °C for 6 h at a heating rate of 1 °C/min.

For the catalyst synthesis by the different methods, the Si/Co molar ratio was kept constant and equal to 10.

The "exchanged material" (Co-MCM-41 EXC) was prepared from the MCM-41 precursor according to the procedure described by Ohtsuka et al. [34]. A mass of $Co(NO_3)_2{\cdot}6H_2O$ (Riedel-de-Haën, ≥97% purity) was dissolved in water up to a Si/Co molar ratio of 10 and then the MCM-41 precursor was added. The mixture was kept under vigorous stirring for 1 h and settled for 12 h at 50–60 °C. Once the contact time was completed, the solid was filtered, washed with distilled water, dried for 12 h at 60 °C and calcined under the same conditions than for MCM-41 (500 °C).

The "impregnated material" (Co-MCM-41 IMP) was prepared from the MCM-41 support. In this case, a mass of the cobalt nitrate hexahydrate was weighted and dissolved in absolute ethanol, using a volume of the solution six times higher than the total pore volume of the sample, according to Concepción et al. [9]. The obtained solution was added drop wise to the MCM-41 and magnetic agitation was applied for 1 h. Afterwards, the solvent was kept for 12 h, until total evaporation of the solvent. Then, precursor was calcined at 300 °C for 5 h at a heating rate of 10 °C/min.

The "incorporated material" (Co-MCM-41 INC) was prepared following a modified procedure of the original technique described by Chanquía et al. [37], using the same molar ratio than the support, TEOS:NaOH:CTAB:H_2O, and adding enough quantity of cobalt salt to the TEOS to obtain a Si/Co molar ratio of 10. Once the salt was added to the TEOS, the NaOH/CTAB solution was added drop wise up to the formation of a gel. Finally, the mixture was stirred for 24 h, then following the same steps of filtration, drying and calcination previously described for the MCM-41 support.

2.2 Characterization

The morphology of the materials was observed by scanning electron microscopy (SEM), using a LEO 1450VP microscope, with a Génesis 2000 EDS system.

The textural characterization was carried out by N_2 adsorption/desorption isotherms (N_2 with 99.999% purity) conducted in an ASAP 2000 (Micromeritics Instruments). Prior to each analysis, the samples were vacuum-degassed at 200 °C and 5×10^{-4} mmHg for 6 h. From the N_2 adsorption/desorption data obtained for each catalyst and support, specific surface area values were estimated by the Brunauer, Emmet and Teller method (S_{BET}) [38] and the total pore volume (V_T) was obtained by the Gurvich's rule [39]. The volume corresponding to the primary mesopores (V_p) was established using the α-plot method as reported by Jaroniec et al. using macroporous silica gel LiChrospher Si-1000 as the reference adsorbent [40, 41]. The pore size distributions were obtained by the NLDFT method for SiO_2 cylindrical pores in the adsorption and desorption branches [42].

The structural characterization of the samples was performed by X-ray diffraction (XRD) in a Philips PW 3830 diffractometer with Cu Ka radiation ($\lambda = 1.5418$ Å) in the range of 2θ from 1° to 10° and from 20° to 80°. The scanning conditions were in steps of 0.01 and at a scan speed of 1 degree/min.

Using the interplanar spacing (d_{100}) (obtained by XRD) and the estimated V_p (volume of primary mesopores) the diameter of the primary mesopores (w_p) were calculated following the procedure described by Kruk et al. [43] applicable to materials with infinite array of cylindrical pores arranged in a hexagonal pattern. The w_p was calculated with the equation:

$$w_p = \left(\frac{8}{\pi \cdot \sqrt{3}}\right)^{1/2} \cdot d_{100} \cdot \left(\frac{\rho \cdot V_p}{1 + \rho \cdot V_p}\right)^{1/2} \quad (1)$$

where w_p is the diameter of primary mesopores, the d_{100} is the planar space obtained by XRD for planes (100), V_p is the volume of primary mesopores and ρ is the density of the amorphous silica (2.2 g/cm^3) considered to be equal to the density of the pore walls [43]. The center-to-center distance between neighbor pores (a) and the pore wall thickness (e) were calculated with the following equations:

$$a = \frac{2}{\sqrt{3}} \cdot d_{100} \quad (2)$$

$$e = a - w_p \quad (3)$$

The quantity of Co in the obtained materials was determined by atomic absorption using a Varian Spectra AA 5.0 and a Co lamp at 345.4 nm of wavelength. The samples were previously digested with aqua regia, HF and $HClO_4$ in a 5:3:3 ratio and diluted in 5% v/v HNO_3.

The assays of temperature-programmed reduction (TPR) were conducted with a gas mixture of 5% H_2 (99.999% purity) in N_2 (99.999% purity) in a Chembet 3000 equipment (Quantachrome Instruments) at a rate of 10°C/min.

X-ray photoelectron spectra (XPS) were obtained in a VG Microtech ESCA apparatus equipped with an Al anode (Al Ka radiation, 1486.6 eV) and VG100AX spherical analyzer. The binding energy was referred to the Si 2p line at 103.4 eV.

2.3 Catalytic Measurements:

Catalytic tests were carried out in Microactivity Reference equipment (PID Eng&Tech. S.L.). About 0.1 g of catalyst was used with a particle size in the range 0.297–0.500 mm for each experiment. The catalytic reaction was carried out in a fixed bed reactor, at 20 bar of pressure, with a ratio H_2/CO = 2, and in the temperature range 170–280 °C. Prior to the catalytic tests, the catalysts were reduced in situ at atmospheric pressure and 400 °C in a gas flow of 10% H_2 in He for 2 h. The products were analyzed on line in a chromatographic system (Perkin Elmer Clarus 500) with three columns: a *Haye Sep* column in series with a *Molesieve 5A* and then in parallel with a capillary column; and two detectors FID and TCD. The heavy hydrocarbons were collected on a condensing system after the analysis. Conversion data were calculated from the CO conversion values. The same catalyst was used in all the temperature range of analysis. Three injections were performed for each temperature and the average value was computed. The analysis time length for each run was about three hours.

3 Results and Discussion

Values of the amount of Cobalt in the catalysts, calculated by chemical analysis and expressed as wt% of Co and Si/Co molar ratio are shown in the Table 1. As observed, samples obtained by the impregnation and the exchange methods, have values slightly higher than 10, which means that part of the Co^{2+} used during the synthesis does not remain on the catalysts. On the other hand, the sample obtained by the incorporation method, presents a Si/Co molar ratio smaller than 10, suggesting that part of the incorporated Co compete with Si atoms in the formation of the material structure.

Figure 1 shows SEM micrographs of the catalysts and the support. As observed, MCM-41 appears to have a soft

Table 1 Chemical analysis of the obtained cobalt catalysts

Sample	Si/Co	wt% Co
MCM-41	–	0
Co-MCM-41 IMP	11.6	7.6
Co-MCM-41 EXC	13.4	6.8
Co-MCM-41 INC	5.4	14.7

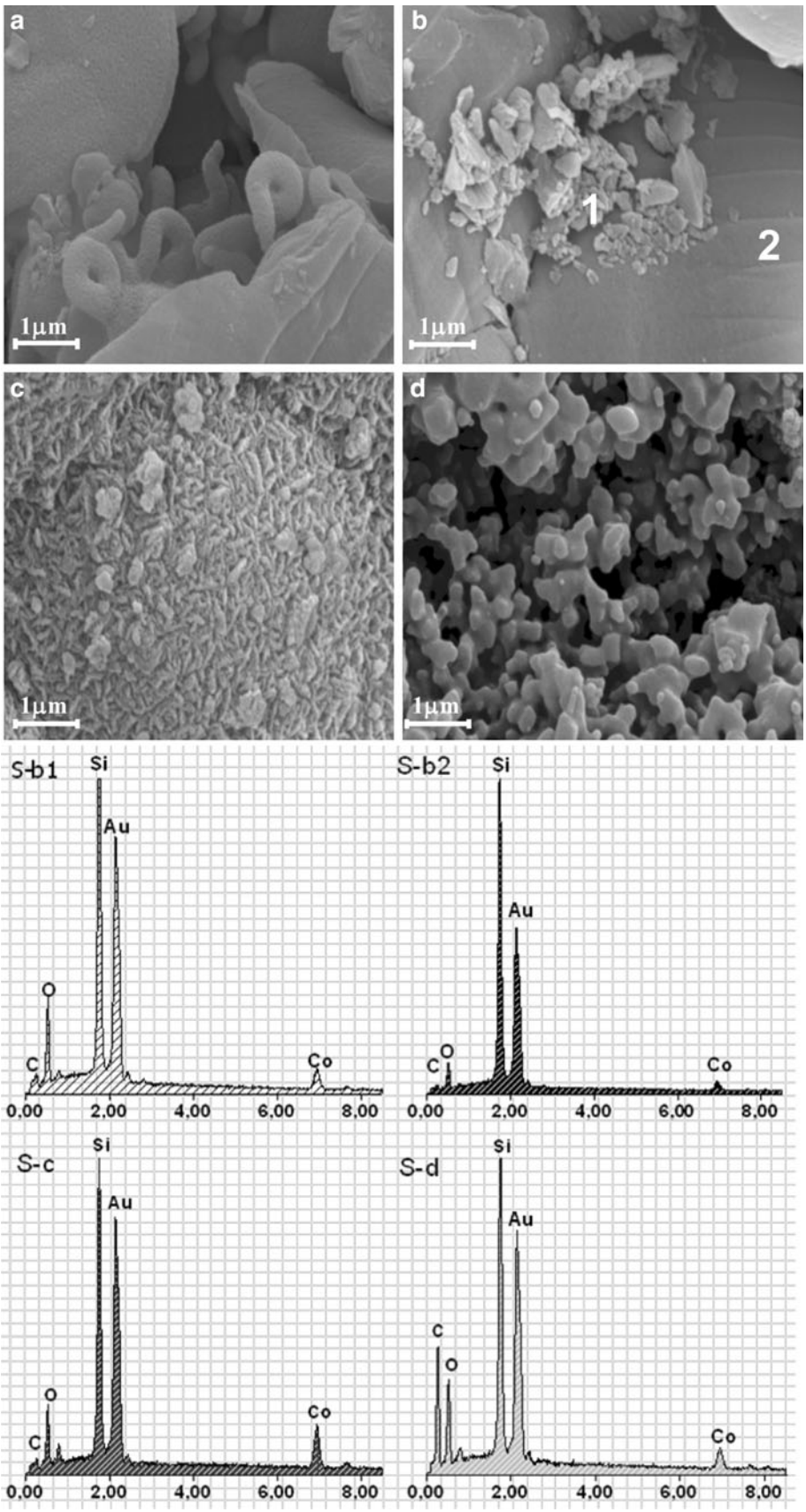

Fig. 1 *Upper figures*: SEM micrographs of the materials (magnification 15000×). **a** MCM-41; **b** Co-MCM-41 IMP; **c** Co-MCM-41 EXC and **d** Co-MCM-41 INC. *Bottom figures*: EDS analysis of different zones of the obtained micrographs. **S-b1** From micrograph b zone 1; **S-b2** From micrograph b zone 2; **S-c** EDS representative of micrograph c; **S-d** EDS representative of micrograph d

surface with some agglomerates of curved rods similar to the ones reported by other authors [44]. Otherwise, the catalysts show a more rugged and intricate morphology. The Co-MCM-41 IMP shows a mixture of soft and rugged surfaces, related to the presence of a silica support and some cobalt oxides deposited outside the MCM-41 structure. The Co-MCM-41 EXC catalyst presents small particles with a lower degree of aggregation compared to MCM-41. It could be noted that agglomerates of curved rods of the support can be also seen at a lower scale. The Co-MCM-41 INC has a soft surface, like the support but a dissimilar morphology to the one shown by MCM-41, with an important degree of particle aggregation. To add some information about these micrographs the EDS analysis was performed. The EDS figures, in the second part of Fig. 1, show that the rough zone has a higher content of Co than the soft regions, in accordance with the above assumptions.

The N_2 adsorption/desorption isotherms carried out for the four materials are illustrated in Fig. 2. As it can be observed, the isotherms of the support and the Co-MCM-41 IMP sample belong to type-IV of IUPAC classification [45], typical of ordered mesoporous materials [9, 25, 39, 42, 46]. Both isotherms show identical shapes although the catalyst has lower adsorption capacity, which would evidence that throughout the impregnation treatment, the support structure remains unchanged, although some pores could become blocked to the nitrogen access.

The isotherm of the Co-MCM-41 EXC sample corresponds to type IIb with a type H3 hysteresis loop, characteristic of the existence of inter-particle pores in aggregates [39]. These results, along with the observations made from the SEM micrographs, would indicate that the solid consists of a large number of aggregates of small particles. The hysteresis shape indicates the presence of pores with several accesses, which would suggest that they are not uniform cylinders.

The Co-MCM-41 INC isotherm exhibits the typical shape of a type IV isotherm, similar to that for MCM-41 up to the capillary region, but showing an important hysteresis loop Type H4. According to previous reports, this loop would correspond to slit-shaped pores, similar to those of pillared clays [39]. However, reported studies on mesoporous materials of MCM-41 type where aluminum has been incorporated, showed that the presence of this hysteresis is due to structural defects within the matrix of the hexagonal arrays [47]. These authors suggested that the framework acquires an enhanced connectivity that improves the catalytic performance of these materials. The hysteresis is due to a percolation phenomenon produced either by the framework interconnectivity, which avoids the evaporation of the N_2 adsorbed within the voids as a result of a pore blocking mechanism, or by a pore blocking caused by imperfections on the mesopores of the material. In both cases, desorption can be exclusively achieved in a coordinated manner at a relative pressure near 0.42. This percolation phenomenon of interconnected pores is also observed in the Co-MCM-41 EXC sample.

It should be noted that the increase of the isotherm slope observed for all the adsorption curves at relative pressures near to 0.3 is related to the capillary condensation occurred within the primary mesopores [30], evidencing their presence in all samples.

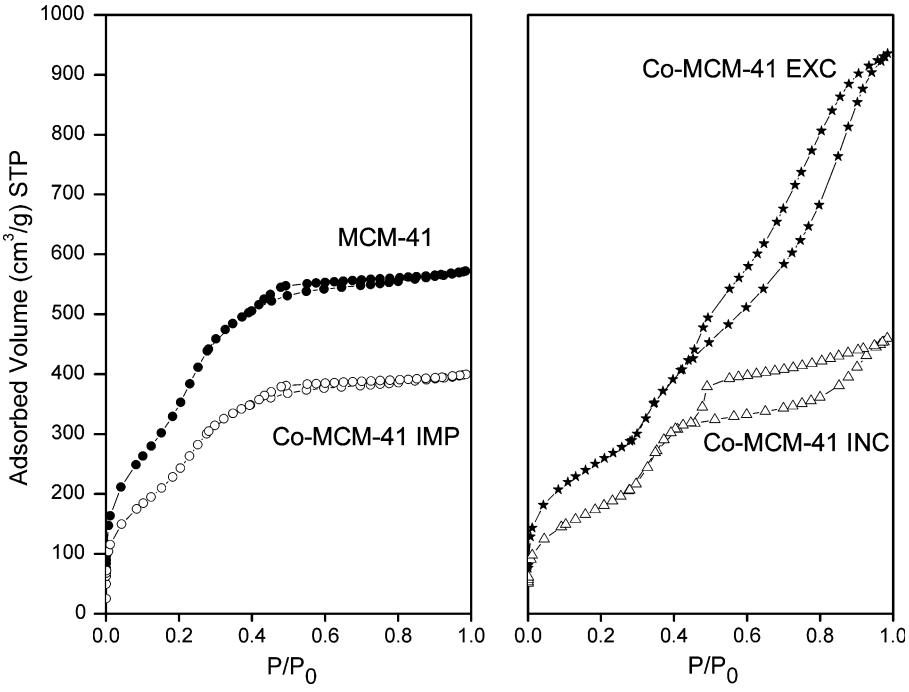

Fig. 2 Nitrogen adsorption–desorption isotherms at 77 K (−196 °C)

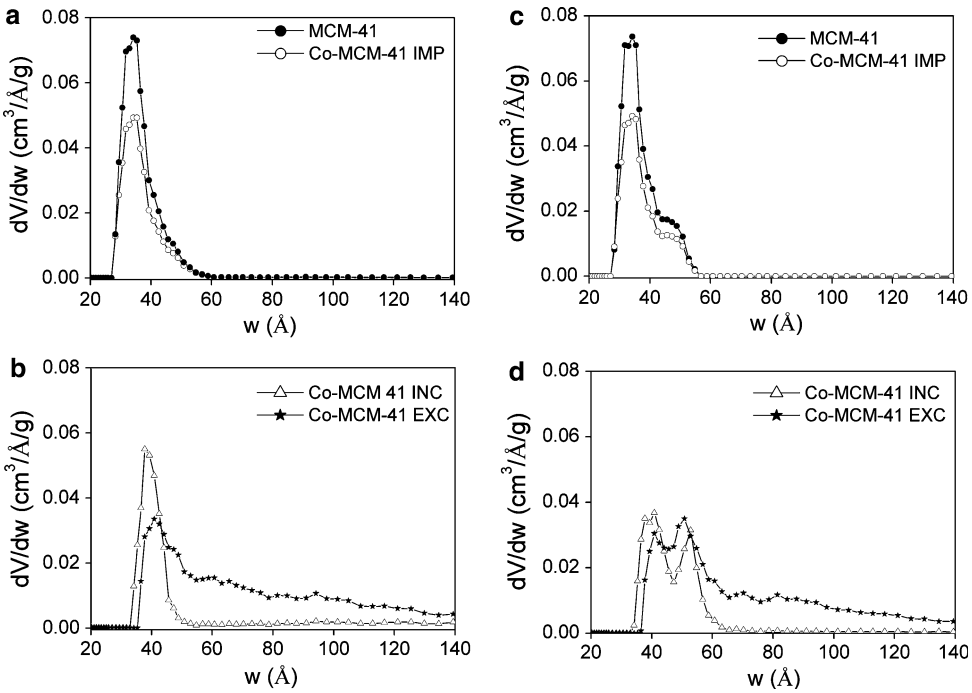

Fig. 3 : PSD of MCM-41 support and Co catalysts. **a** and **b** were calculated employing the adsorption branch, and **c** and **d** with desorption branch

Figure 3 shows the pore size distribution (PSD) of the catalysts and the support, calculated by the Density Functional Theory (DFT) method and using the adsorption branches (Fig. 3a, b) and the desorption branches (Fig. 3c, d). As observed, MCM-41 and Co-MCM-41 IMP materials present a defined pore size of approximately 3.5 nm with a very low contribution of larger pore sizes corresponding to the secondary mesoporosity. The observation concerning to the PSD obtained from the adsorption and desorption branches of the Co-MCM-41 EXC catalyst, evidence a maximum value for pore sizes close to 4 nm for both cases, which would be indicative of the presence of primary mesopores. Furthermore, there is an important contribution of pores having larger sizes (up to 15 nm) caused by the inter-particle pores previously mentioned. The presence of a bimodal PSD calculated from the desorption branch possibly corresponds to a phenomenon of pore blocking and may not be related to pores exhibiting a defined size. The Co-MCM-41 INC sample shows, for the adsorption branch, a PSD with quite defined pore sizes of approximately 4 nm, which corresponds to the primary mesoporosity. This pore size is higher than the exhibited by MCM-41 and Co-MCM-41 IMP samples. This would suggest that the presence of Co in the walls of Co-MCM-41 INC material decreases the known contraction effect undergone by MCM-41 due to calcination. The second peak in the PSD calculated by using the desorption branch corresponds to the percolation originated by the pore blocking effect due to either the imperfections of the catalyst structure or the presence of interconnected pores.

The α-plot obtained from the isotherms for the four materials are shown in Fig. 4, along with the corresponding linear fittings. As it may be seen, the MCM-41 and Co-MCM-41 IMP materials present the same typical behaviour of the MCM-41 mesoporous materials [40]. Besides, the absence of micropores and a low volume of secondary mesopores can also be pointed out. The results obtained for Co-MCM-41 INC show the characteristic adsorption increase that indicates the presence of primary mesopores along with a second step of high slope related to other type of pores, likely caused by the defects present within the material structure. The volume of primary mesopores for the Co-MCM-41 EXC catalyst is difficult to calculate from the obtained α-plot, due to the large growth of the adsorbed volume at intermediate relative pressures, produced by the filling of the inter-particle pores. However, as seen in the PSD plots, this sample presents a contribution of the primary mesopores; then, using a cumulative pore volume until a pore size value of 6 nm, the best linear fitting in an α-plot was estimated, being shown in Fig. 4.

Table 2 summarizes the textural properties of the materials. As it may be seen, Co-MCM-41 IMP catalyst shows a decrease of S_{BET} and V_T values of approximately 30% in comparison MCM-41, as mentioned above. The textural analysis of Co-MCM-41 INC compared to the impregnated catalyst presents a lower value of S_{BET} and a higher value of V_T. This would evidence that the presence of structural defects in the incorporated sample does not contribute to increase the specific surface but the total pore volume. The high S_{BET} value shown by Co-MCM-41 EXC

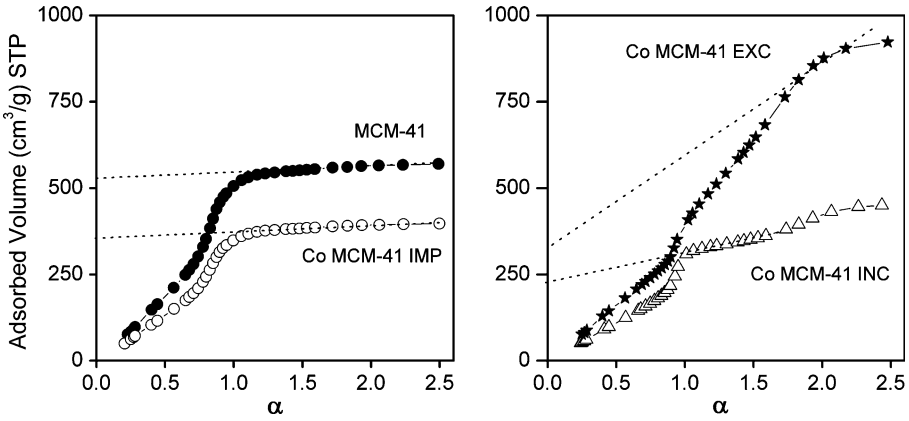

Fig. 4 α-plot curves obtained for MCM-41 and Co catalysts

Table 2 Textural properties of the catalysts and MCM-41

	S_{BET} (m^2/g)	V_p (cm^3/g)	V_T cm^3/g)
MCM-41	1212	0.78	0.89
Co-MCM-41 IMP	840	0.54	0.62
Co-MCM-41 INC	662	0.37	0.71
Co-MCM-41 EXC	934	0.53	1.45

would indicate the presence of primary mesopores, near to 4 nm, as observed in the PSD. Additionally, this sample presents interconnected pores in a continuous and growing size (see isotherms and PSD curves) that difficults the use of the α-plot method for V_p calculation.

The results obtained from X-ray diffraction measurements for the synthesized catalysts and the support at lower angles in 2θ are shown in Fig. 5. The first diffraction peak corresponds to plane (100) of the 2D-hexagonal structure of MCM-41 materials [25, 30, 48]. The weak reflection in the region 4°- 6°, probably due to the overlapping of the diffraction peaks, corresponds to the distance between planes (110) and (200) [37]. For the samples under study, an intense peak of (100) plane was found, typical of mesoporous silica (MCM-41) materials. Therefore, it can be deduced that the materials present a structure with an ordered hexagonal array. Likewise, Co-MCM-41 IMP catalyst exhibits a peak with a very similar shape and identical angle to the MCM-41sample, but with lower intensity. This decrease in the intensity can be attributed to the presence of Co in the matrix, decreasing the number of the hexagonal structures in the impregnated material. For Co-MCM-41 EXC sample a first peak is also present, evidencing the hexagonal array in the material, as shown by the PSD analysis (Fig. 3), corresponding to primary mesopores. However, a shift in the interplanar distance of the material can be observed and seems to be related to the increase of the pore size in accordance with PSD measurements and eventually, to the increase in the pore wall thickness. For Co-MCM-41 INC sample, the broad first

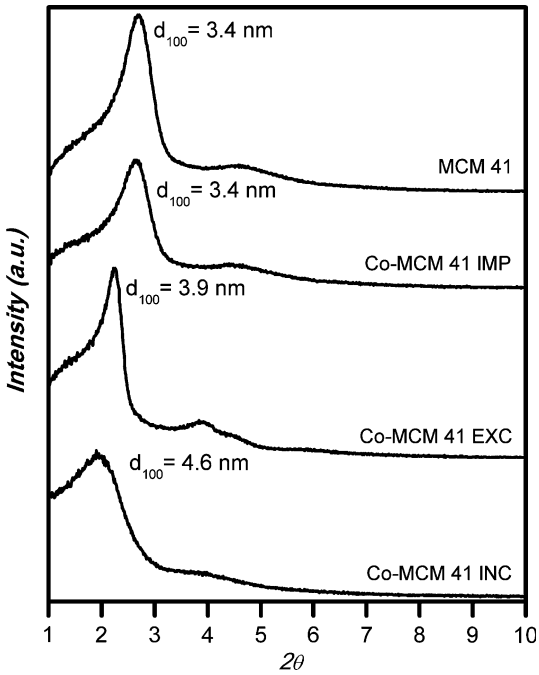

Fig. 5 XRD patterns from 1 to 10° in 2θ of MCM-41 support and Co catalysts

diffraction peak was detected at even lower angles in comparison to the other samples. This displacement can be related to the increase in the wall thickness, as Lim et al. [48] reported for materials with Co incorporated on MCM-41, along with an increase of the primary mesopores size that resulted from the PSD analysis.

From the interplanar distance d_{100} (Fig. 5) and the V_p values (Table 1), the diameter of the primary mesopores (w_d) and the wall thickness (e) values were calculated by using Eqs. 1 to 3. Table 3 summarize these data for all the samples. For the impregnated catalyst it is suggested that cobalt oxide deposition on the support pores causes a decrease in w_d and an increase in e, without changes in the distribution of the channel centres of the hexagonal array. In the incorporated sample, as the cobalt is incorporated

Table 3 Interplanar spacing (d_{100}), size of primary mesopores (w_p) and thickness of the pore wall (e) of the studied samples

	d_{100} (nm)	w_p (nm)	e (nm)
MCM-41	3.4	3.2	0.6
Co-MCM-41 IMP	3.4	3.0	0.9
Co-MCM-41 INC	4.6	3.4	1.8
Co-MCM-41 EXC	3.9	3.5	1.0

during the wall growth of the material, a widening effect of the wall is produced, as shown in this analysis. The presence of Co in the walls of the structure can also reduce the contraction phenomena produced after calcination, obtaining a larger pore size. In the exchanged sample, the surfactant was exchanged by Co after the formation of the silica walls. The subsequent heating treatment of the sample may have induced the incorporation of Co in the walls but from inside the pores, producing a similar effect to the incorporated sample. As shown by the chemical analysis, the cobalt amount is smaller in the exchanged sample than in the incorporated sample, producing a smaller effect on the wall thickness.

From the analysis performed for all the catalysts it is possible to think that all of them maintain part of the hexagonal order of the channels corresponding to MCM-41, but with different values of pore size and pore wall thickness.

Figure 6 shows the X-Ray diffractograms of the catalysts at larger angles. These diffraction patterns show that the impregnated and incorporated samples present Co_3O_4 [34] where the major quantity corresponds to Co-MCM-41-IMP.

In order to study the reducibility of the obtained catalysts, temperature-programmed reduction measurements (TPR) were performed in a 5% H_2 mixture. The results are illustrated in Fig. 7. As observed, the catalyst obtained by impregnation shows two peaks: a first one at approximately 280 °C, typical of Co_3O_4 reduction and a second one at higher temperatures, which is usually related to the reduction of more stable species such as cobalt silicates [9, 19]. Likewise, TPR data obtained for Co-MCM-41 INC show a peak with a lower intensity at a reduction temperature, characteristic for Co_3O_4. At higher temperatures, a more intense peak appears, due to Co oxide strongly linked to the support. This suggests that for this kind of materials, a part the Co is incorporated to the structure but another part can stay as oxide on the surface, possibly leading to additional active sites. Finally, the exchanged sample presents one single reduction peak at high temperatures suggesting that Co deposited by this method is tightly linked to the structure, most likely as silicate species. The results obtained by TPR are in agreement with large angle-XRD results previously mentioned.

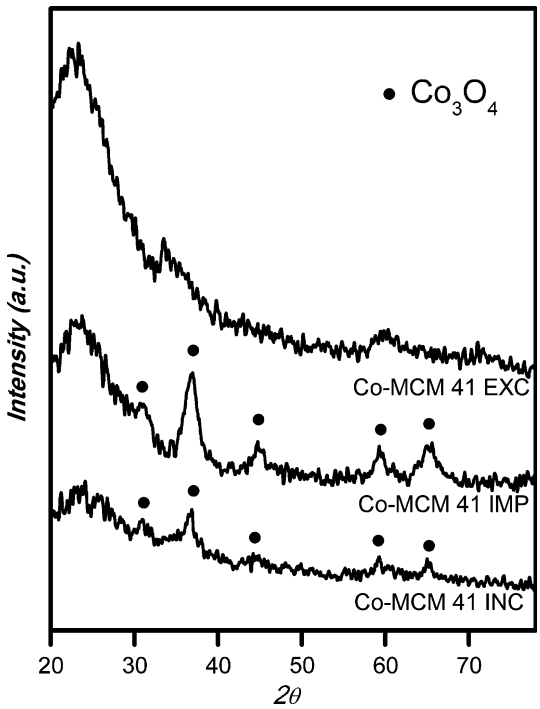

Fig. 6 XRD patterns from 20 to 80° in 2θ of Co catalysts

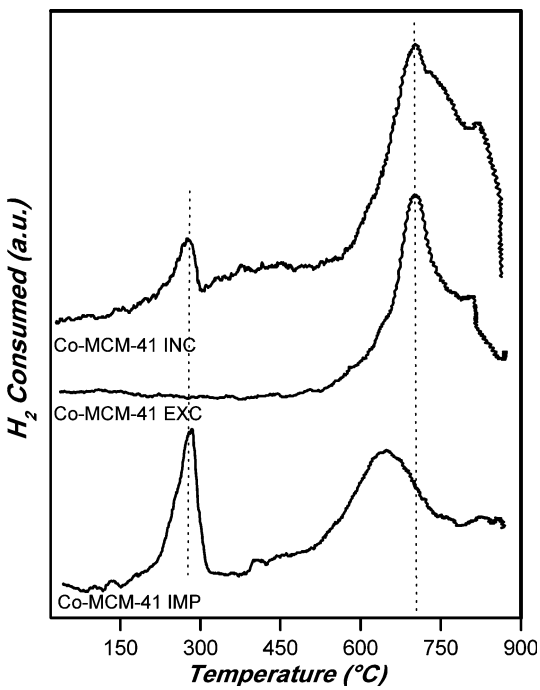

Fig. 7 TPR of the prepared catalysts

Cobalt phases and oxidation states of the catalysts were also explored by XPS. Figure 8 shows the signal of the Co 2p lines. It may be seen that Co-MCM-41 IMP sample exhibits two moderate peaks, which correspond to the Co $2p_{3/2}$ signals at approximately 780 eV and a less intense

signal corresponding to the Co $2p_{1/2}$ at approximately 795 eV, with a spin-orbital splitting of 15.0 eV. The position of these peaks and the magnitude of the splitting are in agreement with values previously reported for Co_3O_4 [2, 24, 49]. In addition, Co-MCM-41 INC sample presents two peaks slightly intense corresponding to the Co 2p that are displaced to higher binding energies, which would correspond to Co^{2+} species like CoO or cobalt silicates [2, 24, 49]. Unfortunately, data from XPS are insufficient to distinguish whether the observed phase corresponds to CoO or other cobalt oxides. Therefore, the TPR analysis is actually the only reliable technique that allows relating the peak displacement to the presence of cobalt silicates [2, 24, 49].

Co-MCM-41 EXC catalyst shows two intense peaks within the spectrum region, as shown in Fig. 8, that are shifted to higher binding energies, close to 781.3 eV, as reported for α-Co_2SiO_4 material [50]. This indicates that cobalt atoms on Co-MCM-41 EXC are strongly linked to the structure and are possibly forming mixed oxides with the silica, as mentioned. However, the high signal intensity of this material is particularly interesting (taking into account that it has the lowest cobalt loading) and can be explained as follows: PSD and XRD data of this material have shown that the hexagonal ordered structure remains in the short range, but not in the long range, where the formation of an intricate array of these basic hexagonal structures occurs, as seen in SEM analysis and shown by

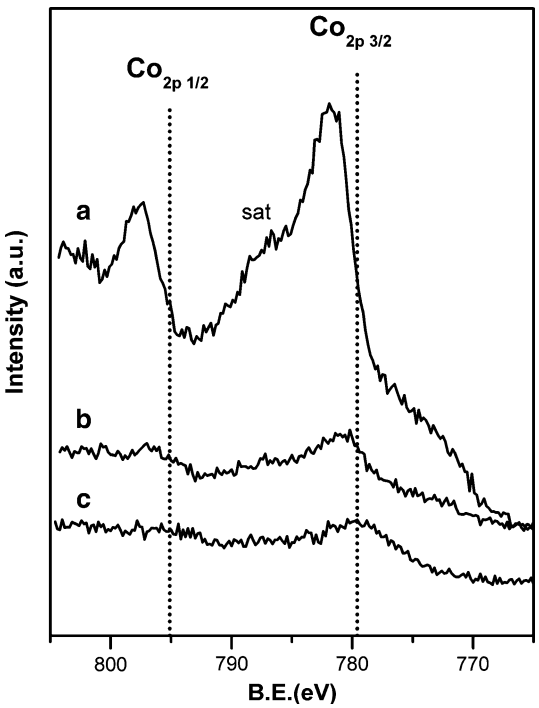

Fig. 8 XPS spectra of the Co 2*p* level for the catalysts: (*a*) Co-MCM-41 EXC; (*b*) Co-MCM-41 INC and (*c*) Co-MCM-41 IMP

the interparticle pore volume deduced from the N_2 adsorption isotherm. Then, although the cobalt loading of this material is smaller, most of it is strongly bounded to the silica and more exposed to the XPS signal.

It is known that catalyst activity in the Fischer–Tropsch synthesis mainly depends on the amount and accessibility of the Co^0 surface sites [2, 6, 9]. Figure 9 shows the intrinsic activity of the catalysts, expressed as mmol of CO consumed per gram of catalyst (a) and per gram of cobalt (b). Figure 9a shows a similar behavior for all catalysts at low temperatures. When increasing the temperature, Co-MCM-41 INC catalyst shows the highest activity, all the rest remaining at a lower similar level. The activity values for the prepared catalysts are similar to those reported in the bibliography and comparatively low due to the low metal loading of the catalysts [9, 34]. Cobalt incorporated-sample has the highest amount of cobalt, according to the chemical analysis, but not all the cobalt is easily reducible (Fig. 7). Therefore, the increased activity of the incorporated-sample catalyst can be attributed not only to the presence of the reducible cobalt but also to its textural properties such as the high surface area and the presence of structure defects (as seen by SEM and N_2-isotherms) that facilitate the accessibility of reactants. A similar catalytic activity was observed for samples obtained by impregnation and ion exchange methods, observing that the impregnated catalyst has the largest amount of easily reducible cobalt oxides, while the ion-exchanged catalyst has the lowest amount of total Co, which is strongly linked to the mesoporous structure. This suggests that some of the surface Co^0 of the ion-exchanged catalyst was formed in the reduction conditions prior to the catalytic test and that the physicochemical properties of this material (high mesopore volume and small size of particle aggregates) contribute to make the Co^0 surface sites more accessible. This would compensate the lower amount of Co and lower reducibility. However, there is no more experimental evidence that support this hypothesis.

When the activity is compared as per gram of cobalt, the behavior is in accordance with the Co loading (Fig. 9b). The incorporated catalyst (Co-MCM-41 INC) presents an activity per gram of Co slightly larger than the other two catalysts at high temperatures (Fig. 9b). This suggests that the temperature is also favouring the access to new active sites. The Co-MCM-41 IMP catalyst shows the lowest activation temperature, due to the larger proportion of easily reducible Co.

Figure 10 shows the distribution of the reaction products for the three catalysts at 280 °C. Co-MCM-41 INC material shows the highest values, although a significant formation of CH_4 in the three cases is related to a low activity. The product distribution is similar for the three catalysts, being slightly higher the formation of C_5+ for Co-MCM-

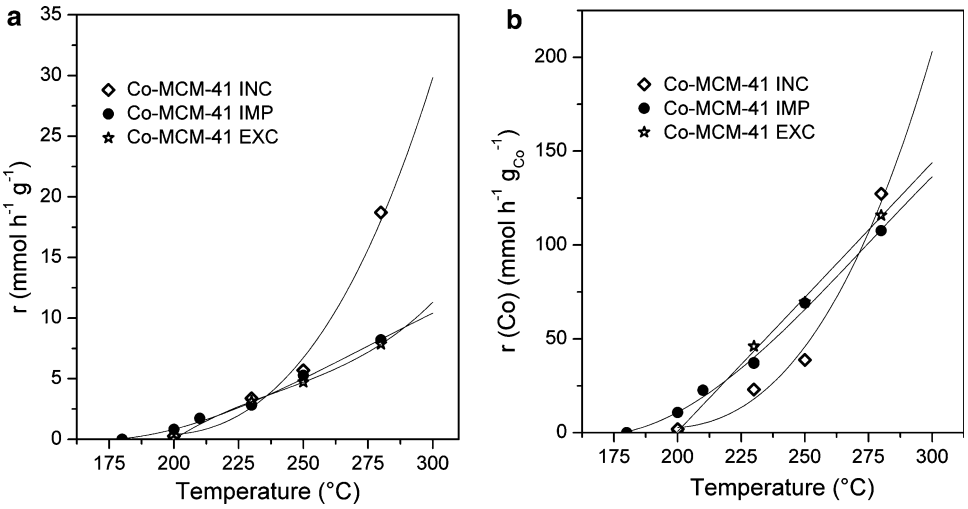

Fig. 9 Intrinsic activity of the catalyst studied at different temperatures **a** per gram of catalyst and **b** per gram of cobalt

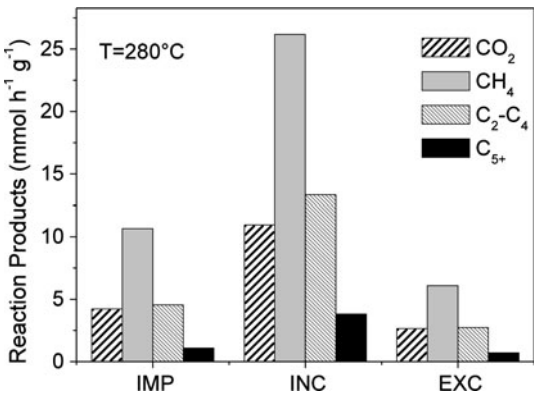

Fig. 10 Reaction products per gram of Co catalysts at 280 °C

41 INC, as a result of a higher production of heavier hydrocarbons [9].

4 Conclusions

Cobalt catalysts based on MCM-41 materials were prepared and characterized. The oxide cobalt precursor was added at different stages of the synthesis process, resulting different catalysts. Cobalt impregnation, direct incorporation and ion exchange techniques were applied, providing the cobalt direct incorporation.

Impregnated catalyst maintains the texture of the basic porous material (MCM-41) and has the largest proportion of reducible species of Co but it is not the most active in the reaction test. The Co species seem to be on the external surface of the material, forming several islands that may be partially blocking the pores.

Exchanged catalyst has a similar amount of cobalt that the impregnated sample, but Co species are strongly linked to Si, which results in larger pores and thicker walls than MCM-41. The texture shows a significant disorder, although the presence of primary mesopores suggests that the basic arrangement of the hexagonal structure is partially maintained, with a significant additional porosity due to interstitial pores. SEM studies show a similar morphology to MCM 41 but the curve rods are much smaller and rougher. The activity of this material is similar to the impregnated catalyst, realizing that not only the number of easily reducible species has a significant contribution, but also the material texture, which plays an important role.

Incorporated catalyst, where Co is directly incorporated to the material walls with a hexagonal arrangement, presents both easily reducible Co species and other Co species strongly linked to the support which may form cobalt silicates. Despite of having a high pore size and the thickest wall for all the samples, this material presents a fairly uniform texture, consisting of primary and secondary mesopores. Secondary mesopores are very important for the allowing the diffusion of reactants and the confinement of the sites, which can increase the activity. This catalyst is the most active, and the product distribution contains heavier hydrocarbons than the other catalysts.

Finally, all the catalysts have different physicochemical characteristics in their morphology, texture and structure that can be related to the activity in the FT reaction.

Acknowledgments The authors gratefully acknowledge Universidad Nacional de San Luis, ANPCyT (Agencia Nacional de Promoción Científica y Tecnológica), Universidad Nacional del Comahue and CONICET for the financial support.

References

1. Vosloo AC (2001) Fuel Process Technol 71:149
2. Khodakov AY, Chu W, Fongarland P (2007) Chem Rev 107:1692
3. Casci JL, Lok CM, Shannon MD (2009) Catal Today 145:38

4. Dry ME (1981) In: Anderson JR, Boudart M (eds) Catalysis Science and Technology. Springer, Berlin, p 159
5. Dry ME (1983) In: Leach BE (ed) Applied Industrial Catalysis 2. Academic Press, New York ch.5
6. Iglesia E, Reyes SC, Madon RJ, Soled SL (1993) In: Eley DD, Pines H, Weisz PB (eds) Advances in Catalysis, vol 39. Academic Press, New York, p 239
7. Iglesia E (1997) Appl Catal A-Gen 161:59
8. Dry ME (2002) Catal Today 71:227
9. Concepción P, López C, Martínez A, Puntes VF (2004) J Catal 228:321
10. Khodakov AY (2009) Catal Today 144:251
11. Tsakoumis NE, Rønning M, Borg Ø, Rytter E, Holmen A (2010) Catal Today 154:162
12. Zhang J, Chen J, Ren J, Li Y, Sun Y (2003) Fuel 82:581
13. Xiong H, Zhang Y, Wang S, Li J (2005) Catal Commun 6:512
14. Song D, Li J (2006) J Mol Catal A-Chem 247:206
15. de la Peña O'Shea VA, Homs N, Fierro JLG, Ramírez de la Piscina P (2006) Catal Today 114:422
16. Panpranot J, Kaewgun S, Praserthdam P (2005) React Kinet Catal Lett 85:299
17. Dutta P, Elbashir NO, Manivannan A, Seehra MS, Roberts CB (2004) Catal Lett 98:203
18. Sun X, Zhang X, Zhang Y, Tsubaki N (2010) Appl Catal A-Gen 377:134
19. Sapag K, Rojas S, López Granados M, Fierro JLG, Mendioroz S (2001) J Mol Catal A-Chem 167:81
20. Su H, Zeng S, Dong H, Du Y, Zhang Y, Hu R (2009) Appl Clay Sci 46:325
21. Martínez A, López C, Márquez F, Díaz I (2003) J Catal 220:486
22. Ohtsuka Y, Arai T, Takasaki S, Tsubocuchi N (2003) Energ Fuel 17:804
23. Xiong H, Zhang Y, Liew K, Li J (2009) Fuel Process Technol 90:237
24. Khodakov AY, Griboval-Constant A, Bechara R, Zholobenko VL (2002) J Catal 206:230
25. Corma A (1997) Chem Rev 97:2373
26. Taguchi A, Schüth F (2005) Micropor Mesopor Mat 77:1
27. Robles-Dutenhefner PA, da Silva Rocha KA, Sousa EMB, Gusevskaya EV (2009) J Catal 265:72
28. Yin D, Li W, Yang W, Xiang H, Sun Y, Zhong B, Peng S (2001) Micropor Mesopor Mat 47:15
29. Li H, Wang S, Ling F, Li J (2006) J Mol Catal A 244:33
30. Khodakov AY, Zholobenko VL, Bechara R, Durand D (2005) Micropor Mesopor Mat 79:29
31. Panpranot J, Goodwin JG Jr, Sayari A (2002) Catal Today 77:269
32. Wei M, Okabe K, Arakawa H, Teraoka Y (2002) React Kinet Catal Lett 77:381
33. Panpranot J, Goodwin JG Jr, Sayari A (2002) J Catal 211:530
34. Ohtsuka Y, Takahashi Y, Noguchi M, Arai T, Takasaki S, Tsubouchi N, Wang Y (2004) Catal Today 89:419
35. Kim DJ, Dunn BC, Cole P, Turpin G, Ernst RD, Pugmire RJ, Kang M, Kim JM, Eyring EM (2005) Chem Commun 11:1462
36. Iwasaki T, Reinikainen M, Onodera Y, Hayashi H, Ebina T, Nagase T, Torii K, Kataja K, Chatterjee A (1998) Appl Surf Sci 130–132:845
37. Chanquía CM, Sapag K, Rodríguez-Castellón E, Herrero EH, Eimer GA (2010) J Phys Chem C 114:1481
38. Brunauer S, Emmett PH, Teller E (1938) J Am Chem Soc 60:309
39. Rouquerol F, Rouquerol J, Sing K (1999) In: Adsorption by powders and porous solids, principles, methodology and applications. Academic Press, New York, ch.1, 13S
40. Sayari A, Liu P, Kruk M, Jaroniec M (1997) Chem Mater 9:2499
41. Jaroniec M, Kruck M, Olivier J (1999) Langmuir 15:5410
42. Ravikovitch PI, Neimark AV (2001) Colloid Surf A 187–188:11
43. Kruk M, Jaroniec M, Sakamoto Y, Terasaki O, Ryoo R, Ko CH (2000) J Phys Chem B 104:292
44. Pauwels B, Van Tendeloo G, Thoelen C, Van Rhijn W, Jacobs PA (2001) Adv Mater 13:1317
45. Sing KSW, Everett DH, Haul RAW, Moscou L, Pierotti RA, Rouquerol J, Siemieniewska T (1985) Pure Appl Chem 57:603
46. Kruk M, Jaroniec M (2001) Chem Mater 13:3169
47. Lin HP, Wong ST, Mou CY, Yang CY (2000) J Phys Chem B 104:8967
48. Lim S, Yang Y, Ciuparu D, Wang C, Chen Y, Pfefferle L, Haller GL (2005) Top Catal 34:31
49. Koizumi D, Hongo Y, Ibi Y, Hayasaka Y, Yamada M (2010) In: Davies B, Ocelli ML (eds) Preparation of highly active Co/SiO_2 catalysts with chelating agents for Fischer-Trospch synthesis—role of chelating agents. CRC Press, Boca Raton, ch. 6
50. Ming H, Baker BC (1995) Appl Catal A-Gen 123:23